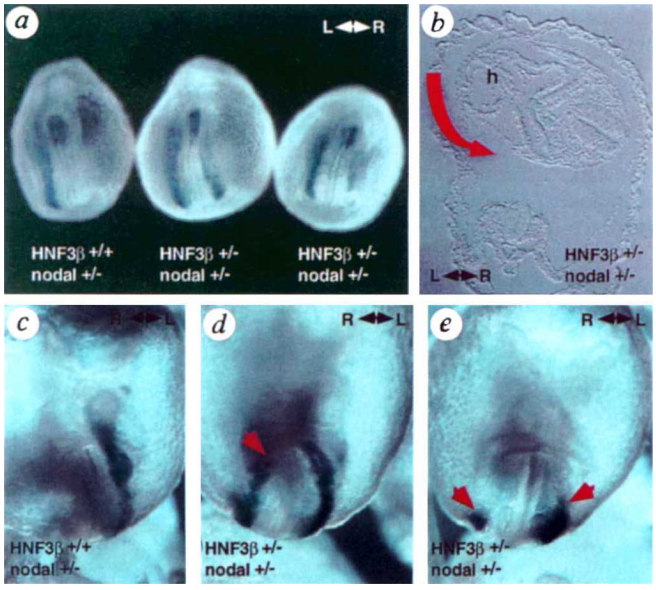

FIG. 4 Misexpression of *nodal* in HNF3-$\beta^{+/-}$ *nodal*$^{lacZ/+}$ double heterozygotes. Embryos were collected at the 8–12-somite stage and stained for β-gal activity. *a*, Posterior views of two HNF3-$\beta^{+/-}$ *nodal*$^{lacZ/+}$ embryos (right) and a *nodal*$^{lacZ/+}$ littermate (left) showing bilateral and left-sided LacZ staining, respectively. Note the differences in the intensity and extent of LacZ staining between these two double heterozygotes. *b*, Transverse section through an HNF3-$\beta^{+/-}$ *nodal*$^{lacZ/+}$ heterozygous embryo showing bilateral LacZ expression associated with a reversal in the direction of turning. The plane of section coincides with the extreme rostral limit of the LacZ staining domain. *c–e*, Frontal views of the embryos shown in *a*, to illustrate the rostral truncation of the *nodal–lacZ* expression domain observed in most of the double heterozygotes.
METHODS. Crosses were established between HNF3-$\beta^{+/-}$ *nodal*$^{lacZ/+}$ males and HNF3-$\beta^{+/-}$ females. Embryos were collected at 8.5 d.p.c. and stained for β-gal activity.

immediately adjacent to the notochordal plate, and a discrete subpopulation of mesodermal cells on the left side of the embryo originating from more proximal regions of the streak. Moreover, the sidedness of *nodal* expression in lateral plate mesoderm predicts the direction of axial rotation and heart looping. Misexpression of *nodal* leads to ambiguities in turning, heart situs and the polarity of the viscera. Thus it seems likely that *nodal* signalling is responsible for highly localized effects on cell migration or proliferation necessary to promote these morphogenetic movements. The *nodal–lacZ* reporter mice described here should allow further evaluation of genetic interactions with other molecular components specifying body situs in vertebrates. □

Received 19 December 1995; accepted 23 February 1996.

1. Kessler, D. S. & Melton, D. A. *Science* **266,** 596–604 (1994).
2. Kingsley, D. M. *Genes Dev.* **8,** 133–146 (1994).
3. Conlon, F. L. & Beddington, R. S. P. *Semin. dev. Biol.* **6,** 249–256 (1995).
4. Conlon, F. L., Barth, K. S. & Robertson, E. J. *Development* **111,** 969–981 (1991).
5. Iannaccone, P. M., Zhou, X., Khokha, M., Boucher, D. & Kuehn, M. R. *Devl Dyn.* **194,** 198–208 (1992).
6. Conlon, F. L. *et al. Development* **120,** 1919–1928 (1994).
7. Beddington, R. S. P. *Development* **120,** 613–620 (1994).
8. Yokoyama, T. *et al. Science* **260,** 679–682 (1993).
9. Levin, M., Johnson, R. L., Stern, C. D., Kuehn, M. & Tabin, C. *Cell* **82,** 803–814 (1995).
10. Zhou, X., Sasaki, H., Lowe, L., Hogan, B. L. M. & Kuehn, M. R. *Nature* **361,** 543–547 (1993).
11. Mountford, P. *et al. Proc. natn. Acad. Sci. U.S.A.* **91,** 4303–4307 (1994).
12. Cooke, J. *Nature* **374,** 681 (1995).
13. Beddington, R. S. P. *J. Embryol. exp. Morph.* **64,** 87–104 (1981).
14. Beddington, R. S. P. *J. Embryol. exp. Morph.* **69,** 265–285 (1982).
15. Lawson, K. A., Meneses, J. J. & Pedersen, R. A. *Development* **113,** 891–911 (1991).
16. Tam, P. P. L. & Beddington, R. S. P. *Development* **99,** 109–126 (1987).
17. Smith, J. L., Gesteland, K. M. & Schoenwolf, G. C. *Devl Dyn.* **201,** 279–289 (1994).
18. Parameswaran, M. & Tam, P. P. L. *Devl. Genet.* **17,** 16–28 (1995).
19. Echelard, Y. *et al. Cell* **75,** 1417–1430 (1993).
20. Chang, D. T. *et al. Development* **120,** 3339–3353 (1994).
21. Marti, E., Takada, R., Bumcrot, D. A., Sasaki, H. & McMahon, A. P. *Development* **121,** 2537–2547 (1995).
22. Ang, S.-L. & Rossant, J. *Cell* **78,** 561–574 (1994).
23. Weinstein, D. C. *et al. Cell* **78,** 575–588 (1994).
24. Poirier, F. & Robertson, E. J. *Development* **119,** 1229–1236 (1993).
25. Hogan, B., Beddington, R., Costantini, F. & Lacy, E. *Manipulating the Mouse Embryo: A Laboratory Manual.* (Cold Spring Harbor Laboratory Press, NY, 1994).
26. Wilkinson, D. G. in In situ Hybridization (ed. Wilkinson, D. G.) 75–83 (IRL, Oxford, 1992).
27. Kaufman, M. H. *Atlas of Mouse Development* (Academic, London, 1992).
28. Neito, M. A., Bennett, M. F., Sargent, M. G. & Wilkinson, D. G. *Development* **116,** 227–237 (1992).
29. Smith, D. E., Del Amo, F. F. & Gridley, T. *Development* **116,** 1033–1039 (1992).

ACKNOWLEDGEMENTS. We thank A. Smith for the IRES-βgeo plasmid; P. Overbeek for the *inv* mice and discussions; D. Bumcrot, E. Marti and A. McMahon for the shh antibody; P. Lewko and M. O'Donnell for animal care; L. Bikoff for comments on the manuscript; and J. Rossant for HNF3-β mutant mice and discussions. This work was supported by postdoctoral fellowships from EMBO, AITPE/CNRS (J.C.) and HFSP (I.V.) and a grant from the NIH (E.J.R.).

CORRESPONDENCE and requests for materials should be addressed to E.J.R.

Conserved left–right asymmetry of nodal expression and alterations in murine *situs inversus*

Linda A. Lowe*, Dorothy M. Supp†, Karuna Sampath‡, Takahiko Yokoyama§‖, Christopher V. E. Wright‡, S. Steven Potter†, Paul Overbeek§ & Michael R. Kuehn*

* Experimental Immunology Branch, National Cancer Institute, National Institutes of Health, Bethesda, Maryland 20892, USA
† Division of Developmental Biology, Children's Hospital Research Foundation, University of Cincinnati, Cincinnati, Ohio 45229, USA
‡ Department of Cell Biology, Vanderbilt University Medical School, Nashville, Tennessee 37232, USA
§ Department of Cell Biology, Baylor College of Medicine, Houston, Texas 77030, USA

VERTEBRATES have characteristic and conserved left–right (L–R) visceral asymmetries, for example the left-sided heart. In humans, alterations of L–R development can have serious clinical implications, including cardiac defects[1]. Although little is known about how the embryonic L–R axis is established, a recent study in the chick embryo revealed L–R asymmetric expression of several previously cloned genes, including *Cnr-1* (for *chicken nodal-related-1*), and indicated how this L–R molecular asymmetry might be important for subsequent visceral morphogenesis[2]. Here we show that *nodal*[3] is asymmetrically expressed in mice at similar stages, as is *Xnr-1* (for *Xenopus nodal related-1*)[4] in frogs. We also examine *nodal* expression in two mouse mutations that perturb L–R development, namely *situs inversus viscerum* (*iv*)[5], in which assignment of L–R asymmetry is apparently random and individuals develop either normally or are mirror-image-reversed (*situs inversus*), and *inversion of embryonic turning* (*inv*)[6], in which all individuals develop with *situs inversus*. In both, *nodal* expression is strikingly affected, being reversed or converted to symmetry. These results further support a key role for *nodal* and *nodal*-related genes in interpreting and relaying L–R patterning information in vertebrates. To our knowledge, our results provide the first direct evidence that *iv* and *inv* normally function well before the appearance of morphological L–R asymmetry.

In the chick embryo, *Cnr-1* is expressed on the left side of Hensen's node beginning at stage 6, but becomes symmetric by stage 9. *Cnr-1* is also found in the left lateral-plate mesoderm (LPM) from stages 8 to 11 (ref. 2). In the mouse embryo, *nodal* expression had previously been studied only at stages before and during early mesoderm formation[3,7]. In contrast to the chick, pre-somite-stage mouse embryos show symmetric *nodal* expression around the mouse node (equivalent to Hensen's node). Using whole-mount

‖ Present address: Department of Anatomy and Developmental Biology, Tokyo Women's Medical College, Tokyo 116, Japan.

in situ hybridization, we examined mouse embryos at stages equivalent to those in chick development when *Cnr-1* is asymmetrically expressed in the LPM. Our analysis revealed that *nodal* expression is asymmetric in the mouse embryo, both around the node and in the LPM. Expression becomes stronger on the left side of the node (Fig. 1*a–c*), a sidedness identical to that shown by *Cnr-1* expression in the chick. Asymmetry was seen as early as the 2–3-somite stage, but a strict correlation between developmental stage and onset of asymmetry is not evident (Table 1). Expression in the left LPM, detected as early as 2–3 somites in a small fraction of mouse embryos, is evident in most embryos by 5–6 somites, but is no longer seen after 9–10 somites (Table 1*a* and Fig. 1). Over this brief period, expression expands from a small region just lateral to the node (Fig. 1*d*), to include the entire LPM (Fig. 1*e*,*h*), then becomes restricted to anterior LPM (Fig. 1*f*), but is not detected in the heart (Fig. 1*g*). We also examined post-gastrulation expression of the three *Xenopus nodal*-related genes[4,8]. Only *Xnr-1* transcripts are detected at these stages, appearing first in a bilaterally symmetric domain flanking the posterior limit of the notochord (Fig. 2*a*), then in the left LPM (Fig. 2*b*,*f*). Spatial changes in the LPM domain of *Xnr-1* expression occur (Fig. 2*c–e*, *g*) that are similar to those seen for *nodal* in the mouse embryo. Whereas there are differences in the expression patterns of *nodal*, *Cnr-1* and *Xnr-1* around the node and notochord in mice, chicks and frogs, the conserved asymmetric LPM expression in these vertebrates suggests that these are cognate genes that might have similar functions in L–R determination.

The best characterized mouse mutations affecting L–R development are *iv* and *inv*.

TABLE 1 Correlation of asymmetric *nodal* expression and developmental age in normal and mutant mouse embryos

(*a*) Normal embryos	Somite numbers									
	0–1	1–2	2–3	3–4	4–5	5–6	6–7	7–8	8–9	9–10
Node										
Symmetric	5	5	4	4	4	5	3	1	1	0
Assymetric	0	4	2	4	9	5	5	8	4	2
No expression								2	8	5
Per cent asymmetric	0	44	33	50	69	50	63	89	80	100
Lateral plate										
No expression	5	7	5	2	1	0	1	8	11	7
Left-side expression	0	2	1	6	12	10	7	3	2	0
Per cent expressing	0	22	17	75	92	100	88	27	15	0

(*b*) Mutant embryos	Somite numbers					
	3–4	4–5	5–6	6–7	7–8	8–9
inv/+ × inv/+	N* N† N†	L† L‡ R*	L† L‡ R* R†§	L† L‡ L† R* L† N† L† N† L†	R* N† L† N† N† N‡ N†	N† N‡ N† N‡ N† N‡
iv/iv × iv/iv	N N R B	N R N B L B	N L N R L R L	N B L B L B R B	N B L B R B	N

In *a*, a compilation of the *nodal* expression pattern of 90 wild-type embryos at different developmental stages (indicated by the number of somites) is shown. Embryos were scored for the pattern of expression around the node and for the presence of LPM expression. For each age group, those showing asymmetric expression around the node are compared to the total with expression around the node, and those showing expression in the left lateral plate are compared to the overall total. Each comparison is given as a percentage. In *b*, the pattern of *nodal* expression in the LPM of individual embryos of different developmental stages and different genotypes is shown. The genotype (if known) of embryos from the *inv*/+ by inv/+ cross is indicated. All embryos from the *iv/iv* by *iv/iv* cross are homozygous. N, no lateral plate expression detected; L, left lateral plate expression; R, right lateral plate expression; B, expression in both lateral plates.

* Genotyped by PCR as *inv/inv*.

† Genotyped as *inv*/+ or +/+.

‡ Unknown genotype (PCR failure).

§ Apparent genotyping error.

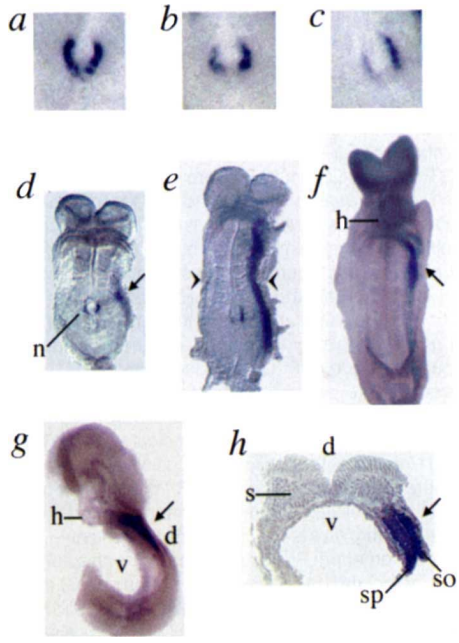

FIG. 1 Analysis of *nodal* mRNA expression in wild-type mouse embryos. In *a–f*, embryos are oriented with anterior to the top and are viewed from the ventral side. Therefore each embryo's left side is toward the right in the figure. Progression to asymmetry around the node is illustrated in close-ups of *a*, a pre-somite embryo; *b*, a 3–4-somite embryo; and *c*, a 5–6-somite embryo. *d–f*, Changing pattern of expression in the lateral-plate mesoderm: *d*, a 4–5-somite embryo with limited expression lateral to the node (arrow); *e*, a 5–6-somite embryo with expression throughout the lateral plate; *f*, a 7–8-somite embryo with mostly anterior expression (arrow). In *g*, a left-side view of a 7–8-somite embryo illustrates that lateral plate expression (arrow) does not extend into the heart (h). In *h*, a cross-section (magnification, ×80) from a 5–6-somite embryo cut at the level marked (arrowheads) in *e*, shown with its left side towards the right of the figure, indicates expression in both splanchnopleure (sp) and somatopleure (so). Other abbreviations: d, dorsal; n, node; s, somite; v, ventral.

METHODS. Gestational-day-eight embryos (BALB/c by Sw) were dissected free of extra-embryonic membranes to lessen lordosis, then fixed and processed for whole-mount *in situ* hybridization as described[22], with modifications. Embryos were hybridized in 50% formamide, 0.75 M NaCl, 10 mM PIPES (pH 6.8), 1 mM EDTA, 0.1 mg ml^{-1} tRNA, 0.1% BSA, 1% SDS and 0.1% Tween-20, and washed in TBST[23]; goat serum was used instead of sheep serum. BM-Purple (Boehringer Mannheim) was used for the colour reaction. The *nodal* antisense probe has been described[3]. Following hybridization, embryos were embedded in plastic and cross-sectioned at 10 microns.

The *iv* mutation results in approximately half of *iv/iv* mice developing with *situs inversus*. In comparison, almost all *inv* mutants show *situs invertus*. We examined *iv* and *inv* mutant embryos at appropriate developmental stages to determine whether these mutations affect the asymmetric expression of *nodal*. For *inv*, because of post-natal lethality of homozygotes, we examined embryos from crosses between heterozygotes and identified *inv* homozygotes using polymerase chain reaction (PCR). Interestingly, *inv* homozygotes consistently express nodal on the opposite side from normal, in the right LPM (Fig. 3*a* and Table 1*b*). Expression around the node was either symmetric or stronger on the right in most homozygotes. However, one did show discordance of node and LPM asymmetry (Fig. 3*a*). The pattern of *nodal* expression in *iv* embryos was complex. Although some had normal expression in the left LPM, most showed altered patterns of expression. These included right LPM expression, expression of *nodal* on both sides, and the complete lack of LPM expression (Fig. 3*b*, *c* and Table 1*b*). Several embryos without detectable expression had between 4 to 6 somites, in the middle of the predicted expression period. No discordance of node and LPM asymmetry was observed in *iv* mutants.

Asymmetric expression of *nodal* provides a valuable L–R marker for understanding the time and mode of action of *iv* and *inv*. Both genes, identified by their effects on visceral *situs* in mice, clearly act upstream of *nodal* and well before the appearance of the first morphological asymmetry. The *iv* mutation, as well as other mutations in mice[9,10] and humans[11] produce randomization of L–R asymmetric structures. A number of experimental embryo manipulations lead to similar effects[12–16]. The finding that the generation of asymmetry can be genetically or experimentally separated from the assignment of a specific handedness has suggested that there are distinct mechanisms for each[5,17–19]. Based on the *iv* phenotype, it has been assumed that the gene's normal function is to bias handedness after asymmetry is established. Therefore, we predicted that half of *iv* mutant embryos would express *nodal* on the left and half on the right. However, more than 50 per cent show bilaterally symmetric expression or no expression at all, suggesting that *iv* also functions in the breaking of initial L–R symmetry. Thus, although these processes are separable, their regulation may be intimately linked. We speculate that *iv* embryos with bilateral or lacking LPM expression, may be similar to experimentally manipulated chick embryos in which Cnr-1 is bilateral or absent[2], and undergo normal but randomly directed heart looping. However, subsequent L–R developmental abnormalities in these embryos might explain the significant fraction of *iv* mice displaying isomerisms and heterotaxia, namely discordance of the sidedness of different organs, such as normal heart *situs* but an inverted stomach and spleen[5,20,21]. In *inv* mutants, *nodal*'s consistent right LPM expression correlates with the high incidence of complete *situs invertus* seen in older *inv* embryos and newborn mice[6]. A small fraction of *inv* mice show

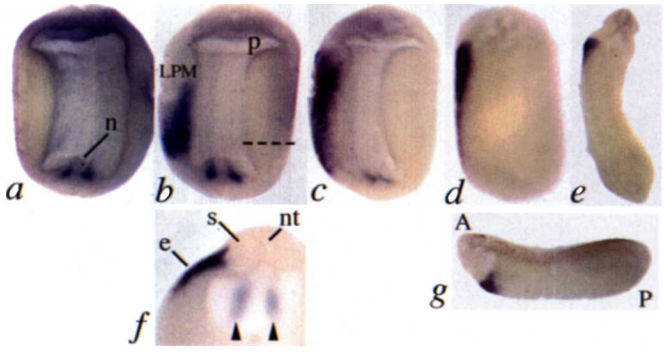

FIG. 2 Analysis of *Xnr-1* mRNA expression in neurula and early tailbud *Xenopus* embryos. In *a*–e, whole-mount stained embryos (nominally, stages 18, 19/20, 21, 22 and 25), were cleared after post-fixing and are viewed dorsally, with anterior oriented to the top of the page. Therefore each embryo's left side is towards the left in the figure. *Xnr-1* expression is down-regulated following gastrulation[4], but reappears during neurulation, first as two bilaterally symmetric patches adjacent to the notochord (n), beginning at stage 18 (*a*) and disappearing after stage 21 (c). A larger domain of *Xnr-1* expression appears in the left LPM from stage 19, first localized in posterior/dorsal mesoderm, and then spreading anteriorly to cover the majority of the LPM (c). Subsequently (*d*, e), *Xnr-1* expression becomes restricted to an anterior/ventral region just posterior of the presumptive heart primordium, adjacent to the developing posterior foregut. In *f*, the embryo in *b* was bisected (as indicated by the broken line), and photographed from an anterior aspect, focusing on the *Xnr-1* signal in the splanchnopleure and somatopleure layers of the LPM. Arrowheads indicate the out-of-focal-plane bilateral expression in the posterior mesoderm. In *g*, a lateral view of the embryo in e is shown to highlight the ventral *Xnr-1* expression. Abbreviations: A, anterior; P, posterior; e, epidermis; LPM, lateral plate mesoderm; n, notochord; nt, neural tube; p, pharyngeal cavity; s, somite.
METHODS. Whole-mount *in situ* hybridization with a full-length antisense *Xnr-1* RNA probe generated from the entire cDNA[4] was carried out essentially as described[24] with minor modifications, including the use of BM-Purple and embryo powder as an additional blocking reagent to reduce background.

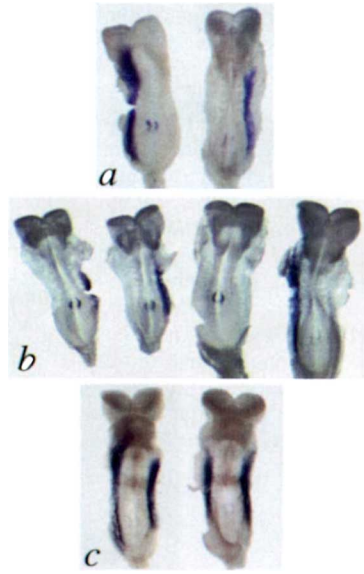

FIG. 3 Analysis of *nodal* mRNA expression in *inv* and *iv* mouse embryos. In *a* and *b*, embryos are viewed dorsally, with anterior oriented to the top of the page. Therefore each embryo's left side is towards the left in the figure. In *a*, two 5–6-somite embryos from an *inv/+* by *inv/+* cross are shown. The embryo with right lateral plate expression is an *inv/inv* homozygote. In *b*, four *iv/iv* embryos are shown: two 6–7-somite embryos with right lateral plate expression; a 3–4-somite embryo lacking lateral plate expression; and a 7–8-somite embryo with normal left lateral plate expression. In *c*, two 6–7-somite *iv/iv* embryos are viewed ventrally (each embryo's left side is towards the right in the figure). Each shows expression of nodal in both the right and the left lateral plates. Note that the extent of expression in the right and left LPM differs in these two embryos, indicating that a degree of L–R asymmetry exists even though these are overtly symmetric for nodal expression.
METHODS. Female mice heterozygous for the *inv* mutation were superovulated and mated to male heterozygotes. Embryos were collected and processed for *in situ* hybridization as described for wild-type embryos. Following hybridization, individual embryos were lysed, their DNA purified and PCR used to amplify either a fragment of the tyrosinase transgene or a fragment of the region deleted in the *inv* mutation. After PCR, reactions were gel-electrophoresed, Southern blotted and hybridized to radioactively labelled probes corresponding to each amplified fragment. Embryos that showed amplification only of the transgene were genotyped as *inv/inv*; all others were genotyped as wild-type or heterozygous. For *iv*, embryos were collected from superovulated SI/COL females mated with SI/COL males or from natural matings of SI/COL animals, and processed as described for wild-type embryos.

heterotaxia. A molecular basis for this might be the discordance of node and LPM asymmetry that was noted in one individual. A low frequency of abnormal expression in the LPM, similar to that seen in *iv* embryos, might also be possible but not yet seen owing to our small sample size.

Determining how *iv* and *inv* normally regulate *nodal*'s non-random asymmetric expression awaits the isolation of these genes, and will be of key importance to the study of L–R development. *Nodal*'s role in subsequent asymmetric morphogenesis must also be established. The evolutionary conservation of *nodal*'s L–R asymmetry supports the hypothesis that this molecule is a critical component of the signalling cascade in all vertebrates that culminates in L–R morphological asymmetries. The expression patterns of *nodal* and *Xnr-1* show a remarkable similarity to each other and to *Cnr-1*, suggesting that a basic genetic framework for L–R patterning has been evolutionarily conserved in vertebrates that have quite different mechanisms of gastrulation. □

Received 12 February; accepted 27 March 1996.

1. Burn, J. *Ciba Found. Symp* **162,** 282–296 (1991).
2. Levin, M., Johnson, R. L., Stern, C. D., Kuehn, M. & Tabin, C. *Cell* **82,** 803–814 (1995).
3. Zhou, X., Sasaki, H., Lowe, L., Hogan, B. L. & Kuehn, M. R. *Nature* **361,** 543–547 (1993).
4. Jones, C. M., Kuehn, M. R., Hogan, B. L. M., Smith, J. C. & Wright, C. V. E. *Development* **121,** 3651–3662 (1995).
5. Layton, W. J. *J. Hered.* **67,** 336–338 (1976).
6. Yokoyama, T. *et al. Science* **260,** 679–682 (1993).
7. Conlon, F. L. *et al. Development* **120,** 1919–1928 (1994).
8. Smith, W. C., McKendry, R., Ribisi, S. J. & Harland, R. M. *Cell* **82,** 37–46 (1995).
9. Metzler, M. *et al. EMBO J.* **13,** 2056–2065 (1994).
10. van der Hoeven, F. *et al. Development* **120,** 2601–2607 (1994).
11. Pansera, F. *Med. Hypoth.* **42,** 283–284 (1994).
12. Yost, H. J. *Development* **110,** 865–874 (1990).
13. Fujinaga, M. & Baden, J. M. *Teratology* **44,** 453–462 (1991).
14. Yost, H. J. *Nature* **357,** 158–161 (1992).
15. Fujinaga, M., Hoffman, B. B. & Baden, J. M. *Devl. Biol.* **162,** 558–567 (1994).
16. Danos, M. C. & Yost, H. J. *Development* **121,** 1467–1474 (1995).
17. Brown, N. A. & Wolpert, L. *Development* **109,** 1–9 (1990).
18. Klar, A. J. *Trends Genet.* **10,** 392–396 (1994).
19. Yost, H. J. *Cell* **82,** 689–692 (1995).
20. Brown, N. A., Hoyle, C. I., McCarthy, A. & Wolpert, L. *Development* **107,** 637–642 (1989).
21. Seo, J. W., Brown, N. A., Ho, S. Y. & Anderson, R. H. *Circulation* **86,** 642–650 (1992).
22. Henrique, D. *et al. Nature* **375,** 787–790 (1995).
23. Hogan, B., Beddington, R., Costantini, F. & Lacy, E. *Manipulating the Mouse Embryo, a Laboratory Manual* 2nd edn 357–362 (Cold Spring Harbor Laboratory, Cold Spring Harbor, New York, 1994).
24. Harland, R. M. *Meth. Cell Biol.* **36,** 685–695 (1991).

ACKNOWLEDGEMENTS. We thank V. Knezevic, S. Mackem, K. Mahon, M. Moos and C. Tabin for help with methodology and for discussions and advice, and L. Vien for technical assistance in the PCR genotyping. Portions of this work were supported by extramural grants from the NIH to S.S.P., P.O. and C.V.E.W.

CORRESPONDENCE and requests for materials should be addressed to M.R.K. (e-mail: kuehnm@dc10a.nci.nih.gov).

Perceived visual speed constrained by image segmentation

Preeti Verghese* & Leland S. Stone

NASA Ames Research Center, Moffett Field, California 94035-1000, USA

LITTLE is known about how or where the visual system parses the visual scene into objects or surfaces. However, it is generally assumed that the segmentation and grouping of pieces of the image into discrete entities is due to 'later' processing stages, after the 'early' processing of the visual image by local mechanisms selective for attributes such as colour, orientation, depth, and motion[1]. Speed perception is also thought to be mediated by early mechanisms tuned for speed[2–5]. Here we show that manipulating the way in which an image is parsed changes the way in which local speed information is processed. Manipulations that cause multiple stimuli to appear as parts of a single patch degrade speed discrimination, whereas manipulations that perceptually divide a single large stimulus into parts improve discrimination. These results indicate that processes as early as speed perception may be constrained by the parsing of the visual image into discrete entities.

We previously measured the human ability to combine speed information from multiple moving stimuli and showed that whereas increasing the number of stimuli improved speed discrimination, increasing the area of a single stimulus by the same factor did not[6] (Fig. 1). These data do not show the classic summation with increasing area that has been reported for grating detection at threshold contrast[7], and for the detection and direction discrimination of the motion of random dots at suprathreshold contrast[8–10]. Thus, the data shown in Fig. 1 appear to be at odds with the view that speed discrimination is determined early, by local speed-tuned mechanisms[2–5]. Such a framework predicts an improvement in discrimination with increasing stimulus size, either due to an increase in the stimulated area within a unit, or in the number of stimulated units.

To explain this surprising lack of summation, we propose that local speed estimates are influenced by the parsing of the image into discrete entities before or concurrently with the combination of speed information across space. Parsing effectively results in a single independent speed estimate per entity. If the speed estimates from each patch are independent samples from a noisy distribution, then in the multiple-patch condition, averaging across patches improves the estimate of speed. However, in the large-patch condition, there is only a single sample whose precision does not change with the size of the patch, and consequently there is no improvement in speed discrimination.

To test this hypothesis, we measured speed-discrimination thresholds using two complementary approaches. In the fusion experiment, we merged multiple gratings until they became a single stimulus, whereas in the fission experiment, we divided a single large grating into multiple stimuli. Our hypothesis predicts that thresholds will increase as multiple gratings merge to one, regardless of how this is achieved. This is contrary to the prediction of early vision models that assume that the visual field is tiled with arrays of specialized detectors that act in parallel and are insensitive to how the image is parsed.

In the fusion experiment, we merged multiple patches in stages as depicted in Fig. 2. In the multiple-patch condition, three grating patches were maximally separated, and had random spatial phase. In the in-phase condition, the three patches were closer and their phase relationship was consistent with three windows on a full-field grating. In the banana condition, the three patches were fused to form a single banana-shaped patch. In the large-patch condition, the stimulus was a single patch three times the area of the patch used in the multiple-patch condition. Speed-discrimination thresholds for the six observers are plotted, normalized to the threshold in the multiple-patch condition. Five of six observers show thresholds that increase as the multiple gratings are fused into a single patch. Thresholds increase when the stimuli are closer and have consistent phase, increase further when they are fused into the banana configuration, and increase further still going from the banana configuration to the large patch.

In the fission experiment, we divided a single large patch and separated the parts as depicted in Fig. 3. In the occluded condition, we superimposed on the large patch a cross that was darker than the background, thus giving the appearance of a single patch occluded by a cross. In the divided condition, we superimposed the same cross but with a luminance equal to the background, thus perceptually dividing the patch into four quadrants. In the multiple-patch condition, four gratings were maximally separated. Speed-discrimination thresholds for the six observers are plotted, normalized to the threshold in the multiple-patch condition. Starting with the large-patch condition, thresholds are unchanged by the occluder for four of our six observers. This result is consistent with the view that the stimulus in the occluded condition is amodally completed[11] and therefore perceived as a single patch moving behind a cross. However, thresholds do decrease in

* Present address: Smith Kettlewell Eye Research Institute, 2232 Webster Street, San Francisco, California 94115, USA.